Biochimica et Biophysica Acta, 693 (1982) 364–378
Elsevier Biomedical Press

BBA 71478

IMAGING VESICULAR DISPERSIONS WITH COLD-STAGE ELECTRON MICROSCOPY

ANDREW H. FALLS [a], H. TED DAVIS [a], L.E. SCRIVEN [a] and YESHAYAHU TALMON [b]

[a] *Department of Chemical Engineering and Materials Science, University of Minnesota, Minneapolis, MN 55455 (U.S.A.) and*
[b] *Department of Chemical Engineering, Technion – Israel Institute of Technology, Haifa 32000 (Israel)*

(Received April 29th, 1982)

Key words: Electron microscopy; Vesicle; Freeze-drying

A fast-freeze, cold-stage transmission electron microscopy technique which can incorporate in situ freeze-drying of the sample is described. Its use in elucidating structure in unstained and stained, hydrated and freeze-dried, aqueous vesicular dispersions of biological and chemical interest is demonstrated with vesicles of L-α-phosphatidylcholine (bovine phosphatidylcholine) and of the synthetic surfactant sodium 4-(1′-heptylnonyl)benzenesulfonate (SHBS). The contrast features observed in transmission electron microscope images of frozen, hydrated samples are identified and explained with the dynamical theory of electron diffraction. Radiolysis by the electron beam is shown to increase contrast in vesicle images and to change their structure and size. Micrographs illustrate the freeze-drying of a dispersion in the microscope; the process causes vesicles to shrink and collapse.

Introduction

A vesicle consists of a closed spherical shell of one or more surfactant bilayers surrounding an aqueous fluid core. An aqueous vesicular dispersion can be formed by sonicating a liquid-crystalline phase that is dispersed in aqueous solution [1]. Vesicular dispersions are translucent and bluish, and contain mostly spherical particles which are 10–100 nm in diameter. Liquid-crystalline dispersions, on the other hand, are turbid and grayish, and contain numerous irregular crystallites which are larger than 0.25 μm. Vesicles serve as model membranes for biochemical research [2,3] and are candidates for drug delivery in the human body [4] and for surfactant delivery in oil reservoirs [5]. Such applications help motivate research on vesicular systems, which also raises important scientific questions.

Abbreviations: DSC, differential scanning calorimetry; SHBS, sodium 4-(1′-heptylnonyl)benzenesulfonate.

Vesicles can be studied with many physicochemical techniques including light-scattering, X-ray scattering, nuclear magnetic resonance spectroscopy, and differential scanning calorimetry (DSC). However, because a model must be used to interpret data from them, these methods can only indirectly reflect structure in a dispersion. In contrast, microscopy directly images the state of aggregation, the shape, and the size distribution of particles in a dispersion. Because the size of vesicles is of the order of scores of nanometers, electron, not light, microscopy is the only means of imaging vesicular dispersions. Electron microscopy, unfortunately, places severe restrictions on samples. For the transmission electron microscope, samples must be thin; the thickness of a typical noncrystalline biological sample is limited by mass-thickness-scattering to about 0.2 μm. In addition, liquid samples must be fixed, that is, their vapor pressures must be dropped below the pressure maintained in the microscope (less than 10^{-6} torr).

A liquid system can be fixed either chemically,

0005-2736/82/0000–0000/$02.75

by adding reagents and drying, or thermally, by rapid cooling; in both cases its original state is altered, the extent of this alteration determining the value of electron microscopy for microstructural analysis. The goal in sample preparation is, of course, to limit structural changes during fixation. Any changes that do occur must be understood so that the appearance of the original system can be reconstructed from images of the altered sample. Because there is always a possibility of introducing artifacts during fixation, it is necessary to vary systematically the sample preparation method before drawing any conclusions about the microstructure in a liquid system. Furthermore, it is desirable to contrast and compare the results of at least one other sample preparation method as well as evidence from less direct probes such as light-scattering and X-ray scattering; DSC is often a useful aid in interpreting images of thermally fixed specimens.

To begin, we point out the advantages and difficulties of the methods commonly used to prepare vesicular systems for the transmission electron microscope. We then describe a new technique for elucidating structure in vesicular dispersions: fast-freeze, cold-stage microscopy which can be combined with in situ freeze-drying. We apply these techniques to aqueous vesicular dispersions and interpret the images of frozen, hydrated systems by the dynamical theory of electron diffraction. Finally, we identify some of the artifacts that can confuse interpretation of the images of both frozen, hydrated and freeze-dried specimens.

Transmission electron microscopy preparation methods

In early work, negative staining followed by drying was used to fix vesicle systems. Horne and Whittaker [6] used potassium phosphotungstate to stain synaptic vesicles without prior fixation. Staining was following by drying which, they claimed, formed "a glass of electron-dense phosphotungstate in which the subcellular particles show up as areas of relatively low electron density". Finean and Rumsby [7] pointed out that structure can change during evaporation and that fixation by osmium tetroxide or potassium permanganate before drying is essential to prevent artifacts. Nevertheless, Horne et al. [8] and Bangham and Horne [9] asserted that the setting of phosphotungstate glass suppresses structural artifacts during drying; they published micrographs that were corroborated by X-ray scattering. Papahadjopoulos and Miller [10] described negative staining, with ammonium molybdate, and drying, but did not address artifacts of specimen preparation. Later on, Glauert and Lucy [11] concluded that phospholipid systems are unaffected by drying but can be altered by stain. Talmon [12] recently showed that staining and drying some amphiphilic systems can actually produce 'bilayered' structure in them. Johnson et al. [13] addressed vesicle collapse upon drying. Another variant of the stain-dry method incorporates a heavy-metal salt [14] or oxide [15] inside the vesicle. This method may also suffer drying artifacts.

Vesicles have been fixed by chemical reaction, e.g., with osmium tetroxide the reagent, as in the work of Miyamoto and Stoeckenius [16], who compared the results with those from staining and drying. They found that the sizes of vesicles fixed with osmium tetroxide were in accord with light-scattering observations from unfixed samples but differed from the sizes of vesicles that were stained and dried. Their study argues for fixing vesicular systems with osmium tetroxide prior to drying them.

Aqueous vesicular dispersions have been fixed thermally as well as chemically. Taylor [17] viewed lipopolysaccharide vesicles, frozen in liquid nitrogen, with cold-stage microscopy. Forge et al. [18] froze dispersions of egg phosphatidylcholine vesicles, placed on copper support discs, in liquid Freon 22. They prepared thin replicas of the frozen specimens and examined them in the electron microscope. Van Venetië et al. [19] also applied the freeze-fracture-replication method to vesicular dispersions, but froze their samples by spraying them into liquid propane [20]. Cooling rates in the spray-freeze method (over 5000 K/s [19]) are higher than those in standard freezing techniques (about 800 K/s [21]). Recently, we showed that thin, frozen vesicle samples can be imaged directly with fast-freeze, cold-stage transmission electron microscopy [22–24]. In this technique, which is described in the next section, cooling rates are of the order of 10^4 K/s [25,26].

Like chemical fixation, thermal fixation is subject to artifacts, most notably those due to phase separation or solute redistribution during solidification. It appears, however, that thermal fixation preserves microstructure in dilute, aqueous vesicular dispersions: vesicles do not agglomerate in transmission electron microscopy samples prepared with either freeze-fracture-replication [18,19] or fast-freeze, double-film techniques [22–24]. Instead, vesicles homogeneously distribute inside single ice crystals and do not concentrate at grain boundaries. Furthermore, variable-temperature ^{23}Na nuclear magnetic resonance spectra and DSC thermograms indicate that surfactant in vesicles remains in single bilayers even when the sample is frozen slowly (at 5 K/s in DSC) [24]. Thus, thermal fixation is apt to preserve vesicle structure.

Frozen, hydrated specimens: preparation and materials

Thin, frozen, hydrated (i.e., undried) specimens for cold-stage microscopy are prepared by trapping a thin layer (ideally less than 0.5 μm thick) of liquid deposited from a syringe between two polyimide film-covered electron microscope grids. Polyimide films, 20–40 nm thick, are used as substrates because they are wet by either oleic or aqueous phases and are radiation resistant [27]. The specimen 'sandwich' is frozen by plunging it into liquid nitrogen and is stored under the cryogen until it is transferred into the microscope. Preparation of polyimide films and specimens as well as observations of well-characterized systems of plasticized latex spheres have been detailed previously [28].

Fast-frozen, thin sample films are not of uniform thickness. Capillary forces, hydrodynamic forces, and quite possibly disjoining pressure effects [29] produce areas of uneven thickness while the sample is drained before it is frozen. Moreover, particles can be fractionated by size during sample preparation so that the distribution of vesicle sizes in a frozen sample may not accurately reflect the distribution in the unfrozen dispersion.

After they are made, frozen samples are transferred into a JEOL JEM 100CX electron microscope cooling-holder equipped with a special cold-stage transfer module [22]. The cold-stage transfer module permits transfer of the holder which contains the frozen specimen into the electron microscope without excessive heating of or frost depositing onto the specimen. The cold-stage transfer module has been modified recently [30].

Once in the microscope, the frozen, hydrated sample on the cold-stage is kept at about 100 K by using liquid nitrogen as the coolant for the stage. Of late, the cooling holder has been altered to contain a controllable heater near the specimen tip [30]; this allows the specimen temperature to be maintained anywhere between 100 and 300 K for long periods of time without introducing thermally induced instability. Micrographs in this paper were recorded in the conventional transmission mode with 100 kV electrons.

Vesicles dispersed in doubly distilled water were prepared from bovine brain phosphatidylcholine and from a synthetic double-tailed surfactant, sodium 4-(1′-heptylnonyl)benzenesulfonate (SHBS) of molecular weight 404.6. The phosphatidylcholine was L-α-phosphatidylcholine prepared chromatographically by the Sigma Chemical Company. SHBS was obtained from the University of Texas and purified by extractions with chloroform and a 95 : 5 (v/v) solution of isobutanol and water [31]. Sodium chloride, cesium chloride and uranyl acetate were certified A.C.S. from Fisher Scientific.

Aqueous liquid crystalline dispersions of the amphiphiles were sonicated until they turned opalescent (15–30 min) in either a Cole-Parmer Ultrasonic bath, model 8845-3, or a Buchler 75-1980 Ultramet III. The water bath temperature was maintained below 310 K. Microscope specimens were prepared within 10 minutes after sonication was halted.

Stained vesicular systems were prepared either by adding stain solution to the dispersion before sonication or by allowing the sonicated dispersion to equilibrate with the stain solution through a semipermeable membrane. Stain was not added directly to a vesicular dispersion because osmotic pressure differences may rupture vesicle bilayers [32].

Contrast in frozen, hydrated vesicular dispersions

Interpreting micrographs requires understanding the electron-optic contrast mechanisms which produce intensity variations in an image. Here we outline the dynamical theory of electron diffraction [33] which is used below to analyze trasmission electron microscope images of frozen, hydrated vesicular dispersions.

Contrast in focussed images of unstained, dried vesicle systems is low because the mass densities of vesicles and the films used to support them are nearly equal. Stains enhance mass-thickness contrast. Positive stains increase electron scattering from vesicle bilayers by replacing the counterion which is ionically bound to the amphiphile with a heavier one. Negative stains, on the other hand, increase the mass density of the continuous phase relative to that of the vesicle bilayers. Negative stains are excluded from amphiphile head-groups by charge.

Staining a dispersion also heightens the contrast factor for X-rays scattered from vesicles. Adding stain to a system, however, can change the microstructure and phase behavior of the surfactant dispersion [24] and affect vesicle size. For example, 1 wt% SHBS sonicated in distilled water forms vesicles that have a z-averaged diameter, according to quasielastic light-scattering measurements, of 45 nm; the z-averaged particle diameter in a 1% SHBS, 1% uranyl acetate dispersion as measured by small-angle X-ray scattering is, however, 25 nm. Thus, data from stained vesicular dispersions should always be compared to that from unstained ones at comparable ionic strengths.

Phase contrast can sometimes be used to image structures that display low mass-thickness contrast. Phase contrast is increased by under-focussing the image. Optimum defocus for a particular structural detail can be estimated from transfer theory [34]. These techniques have been used recently to elucidate structure in unstained lamellar block copolymers with small intrinsic density differences between the phases [35].

In the double-film technique, dilute, aqueous vesicular dispersions freeze into crystalline solid; vesicles become encased in ice grains, the crystal structure of which is hexagonal [36]. The ice matrix also contains grain boundaries, stacking faults, and dislocation defects which have been identified in pure ice samples [26,36]. Because densities of organic molecules and ice differ little, transmission electron microscope image contrast from unstained biological material embedded in crystalline ice must be due primarily to diffraction contrast [17]. In passing through a crystalline solid, an electron beam splits into transmitted and diffracted parts. The intensities of the two parts vary inside the crystal and depend on depth in the crystal, crystallographic orientation of the sample, crystal lattice defects, and inclusions or strain fields. Contrast, which is defined as the difference between the intensities from the background and the inclusion divided by the background intensity, results from excluding various beams with an aperture inserted in the back focal plane of the microscope's objective lens. When the transmitted beam is selected, a 'bright-field' image is formed. When a diffracted beam is selected, a single-beam 'dark-field' image is formed.

Amplitude contrast in images from an ideal, focussed microscope, that is, one in which the microscope transfer function [34] is unity inside the objective aperture and zero otherwise, is accounted for by the dynamical theory of electron diffraction [33]. The two-beam approximation to the theory, in which diffuse small-angle scattering and weakly excited Bragg reflections are neglected, provides qualitatively correct explanations of transmission electron microscope images. Calculations from the two-beam theory best describe experimental images that are formed when only a single diffracted beam is strongly excited. Unfortunately, true two-beam conditions cannot be obtained in the microscope because the geometrical conditions for diffraction of high-energy electrons are nearly satisfied for a number of reflections simultaneously.

The theoretical treatment of the contrast of a vesicle embedded in ice follows that of an inclusion [37] or a void [38,39] in a crystalline metal. The contrast variation throughout the projected image of the inclusion is obtained by applying the equations of the dynamical theory [33] to a series of columns in the crystal, each passing through a different cross-sectional thickness of the inclusion. To calculate intensity distributions in transmission electron microscope images of frozen vesicular dis-

persions, ice absorption lengths, vesicle extinction and absorption distances, specimen and vesicle thicknesses, and Bragg deviation parameters are needed. The ice normal absorption length, ξ'^{ice}_0, scales intensity in the calculated image. Contrast profiles are more sensitive to the ratio of the anomalous absorption length to the diffracted beam extinction distance, ξ'^{ice}_g/ξ^{ice}_g, which is a strong function of temperature, the diffraction vector $\boldsymbol{g}$, and objective aperture size [40].

Absorption lengths in ice have not been measured; extinction distances and absorption lengths inside a vesicle are even more difficult to obtain because radiation damage intrudes. As a result, we treat unstained vesicles as amorphous inclusions ($\xi^{ves}_g = \infty$, with $\xi'^{ves}_0 = \xi'^{ice}_0$) in ice that is described by absorption parameters characteristic of crystalline materials ($\xi'^{ice}_0/\xi^{ice}_g = \xi'^{ice}_g/\xi^{ice}_g = 10$). To describe stained systems, we decrease ξ'^{ves}_0 to $\xi'^{ice}_0/3$. With these parameters, calculated contrast profiles explain transmission electron microscope images of frozen vesicular dispersions.

Experimental Results and Discussion

Structure in frozen, hydrated vesicular systems

Fig. 1a is a micrograph of a 1% SHBS, 0.1% NaCl sonicated dispersion. The spherical particles, 25–90 nm in diameter, are vesicles lying within a single ice crystal. The larger particle in Fig. 1a is a liquid-crystallite; even after prolonged sonication, a few liquid-crystalline particles remain in the dispersion. These crystallites can bias the average vesicle size measured by light-scattering or small-angle X-ray scattering [24]. Fast-freeze, cold-stage transmission electron microscopy determines the presence of small (under 0.5 μm) liquid-crystalline particles in a dispersion even when visual observations, spectroturbidimetry, light-scattering and X-ray scattering cannot.

Fig. 2 is an image from an unstained, frozen, hydrated specimen of 0.08%. bovine phosphatidylcholine sonicated in distilled water. Vesicles appear either dark (A) or light (B) against the ice in which they are embedded, depending on the thickness of the ice crystal and its orientation. Long-ranged strain fields produce local variations in the orientation of ice crystal planes. The appearance of a vesicle changes as the local Bragg condition varies. The difference is negative versus positive contrast and can be understood with the dynamical theory of electron diffraction: Fig. 3, called a rocking curve [41], shows the calculated variation in contrast at the center of a vesicle's transmission electron microscopic image as the Bragg conditions of the crystal containing the particle change. The profile in Fig. 3 is for a vesicle located midway through an ice crystal of uniform thickness. Depending on the diffracting conditions, the center of the image appears dark (negative contrast) or light (positive contrast).

Some vesicles in Fig. 2 (at (C) for instance) appear as a bright inner area surrounded by a dark ring. This too can be explained by diffraction contrast theory. Fig. 4 shows the contrast calculated for the projected image of a vesicle. Close to its edges, this particle displays negative contrast. Near its center, the image is lighter.

Although unstained vesicles can be imaged by cold-stage microscopy [22–24], their contrast in thicker sample areas (more than 0.25 μm thick) is usually low. (Structures producing contrast levels below about 10% are invisible in a micrograph.) Stain increases electron-scattering from vesicles and enables features that are invisible in unstained dispersions to be imaged. Fig. 5, which is a $(10\bar{1}0)$ dark-field image of a frozen, hydrated specimen of a 1% SHBS dispersion sonicated in 1% uranyl acetate solution, is an example. $(10\bar{1}0)$ is standard hexagonal crystal lattice notation [42] and denotes the diffracted beam used to form the dark-field image. The ice crystal in Fig. 5 contains a uranyl acetate-stained SHBS liquid-crystalline particle (A) and numerous stacking fault fringes (B) [26]. The alternating intensity extrema (C), called 'thickness fringes' [41], are lines of constant thickness in the crystal. The difference in thickness between one fringe and the next is one extinction distance, ξ^{ice}_g (equal to 200 nm for the $(10\bar{1}0)$ reflection [26]). If the crystal is near the exact Bragg condition, the total thickness at a point in the ice crystal can be estimated by counting thickness fringes. Near the top of Fig. 5, the matrix is thin (less than one extinction distance). At the bottom of the figure, the crystal thickness is greater than 1 μm. Because stain is present, vesicles are visible in these areas.

In Fig. 5, some vesicles of nearly the same size, e.g., those at (D), differ in contrast as the thickness

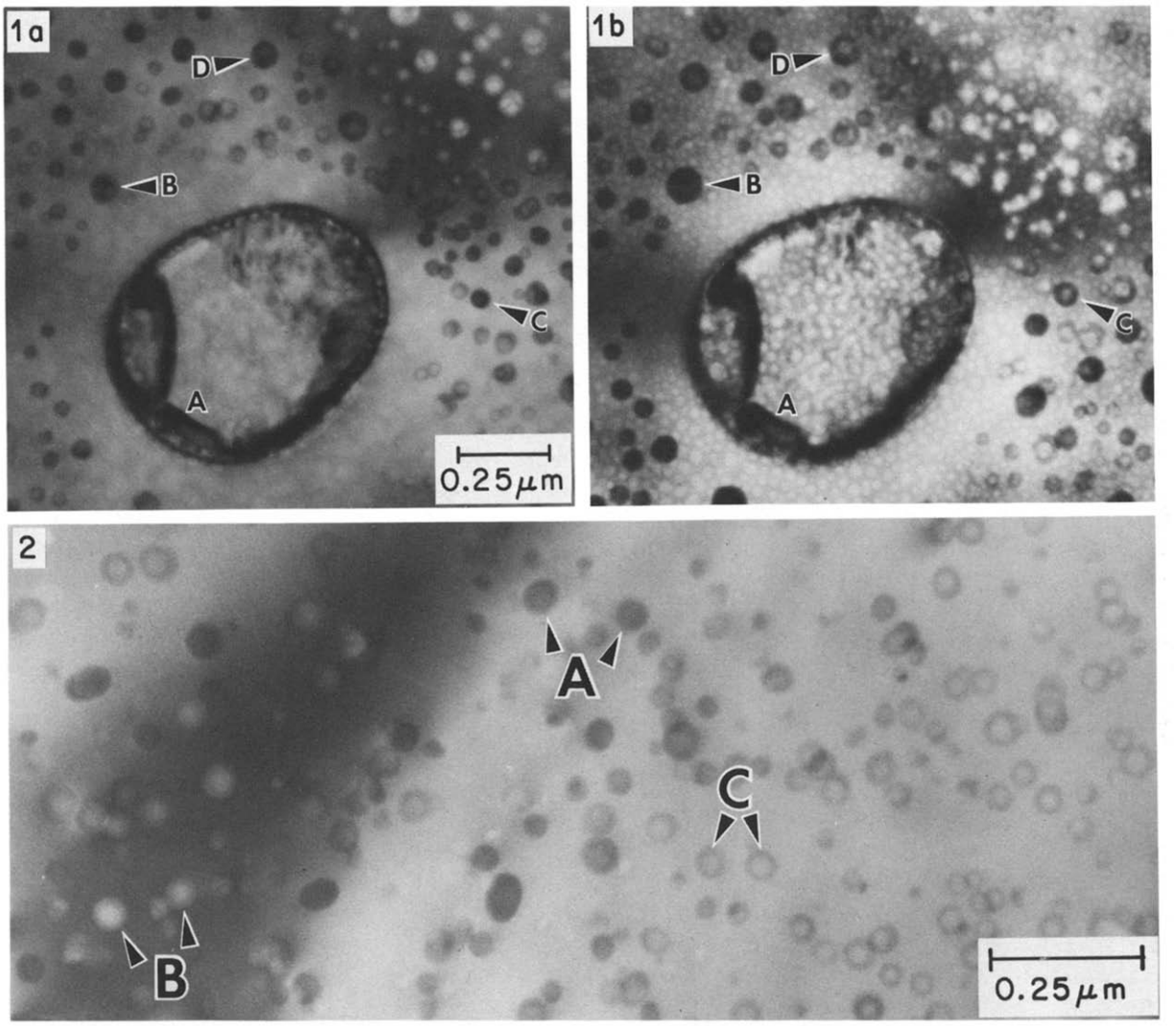

Fig. 1. a. Bright-field micrograph of an unstained, frozen vesicular dispersion of 1% SHBS in 0.1% NaCl brine. A large liquid crystallite (A) is present in the dispersion. b. Area in a after receiving an additional electron dose of $4 \cdot 10^3$ C/m^2. During radiolysis some vesicle images (e.g., at B) expand, others (C) get areas of lower contrast on them, and some appear lighter (D) or disappear.

Fig. 2. Bright-field micrograph from an unstained, frozen, hydrated vesicular dispersion of bovine phosphatidylcholine. Vesicles display both negative contrast (e.g., at A) or positive contrast (B) over the ice matrix. Some vesicles (C) appear as a bright inner area surrounded by a dark ring.

of the ice increases. Other vesicles, at (E) for instance, differ in contrast even though the ice thickness is uniform. The appearance of larger vesicles (F) differs from that of smaller ones (E). These contrast features can be understood with the dynamical theory. Fig. 6 shows calculated bright-field and dark-field contrast profiles for the center of the image of a vesicle located midway through ice crystals of increasing thickness. The contrast may be negative (dark) or positive (light). In thicker crystals, vesicle contrast is low. Figs. 7 and 8 illustrate that the appearance of the vesicle center is a function of both its size and position in a crystal of uniform thickness.

In SHBS systems, uranyl acetate behaves as a positive stain. The density of vesicle bilayers in-

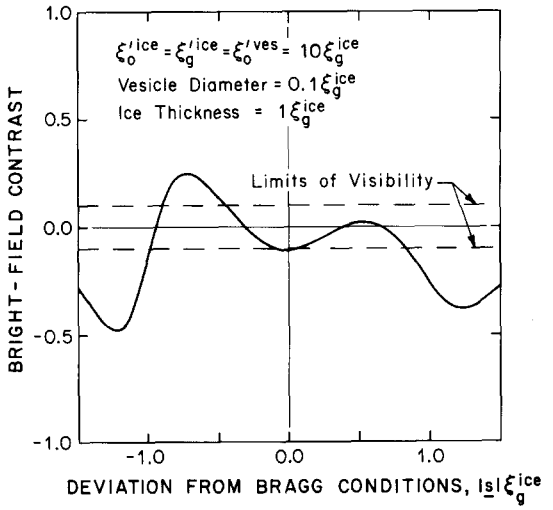

Fig. 3. Calculated bright-field contrast at the center of the image of a vesicle located midway through an ice crystal as a function of the deviation of the ice crystal from the exact Bragg diffracting condition. Vesicles change their contrast as the diffracting conditions vary and can appear either dark or light.

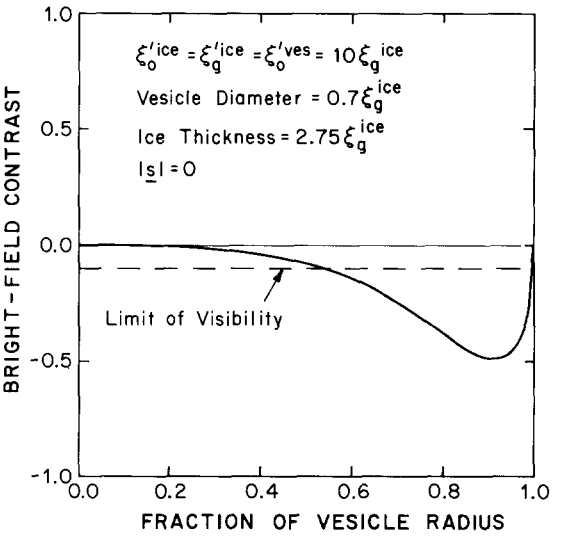

Fig. 4. Calculated variation in bright-field contrast throughout the image of a vesicle. The inside of the vesicle is brighter than its edges.

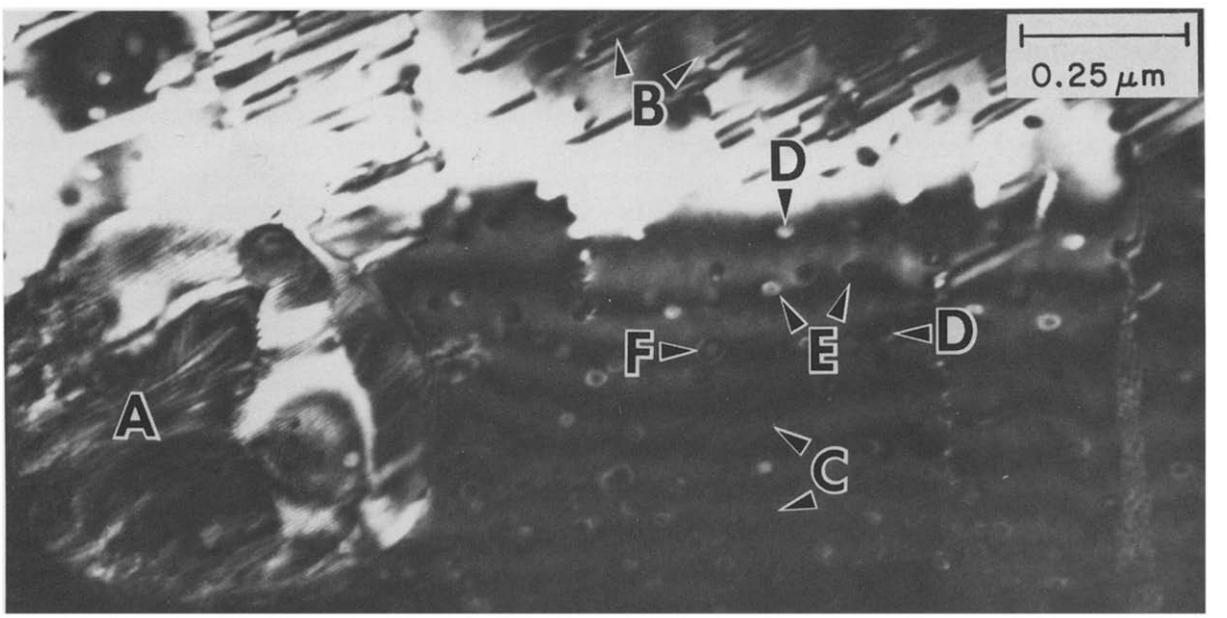

Fig. 5. ($10\bar{1}0$) dark-field image of a frozen, hydrated 1% SHBS dispersion sonicated in 1% uranyl acetate. A liquid-crystalline particle (A), stacking faults (B), and thickness fringes (C) are visible. Vesicle contrast depends on the ice thickness (D), vesicle depth within the crystal (E), and vesicle size (compare E, F).

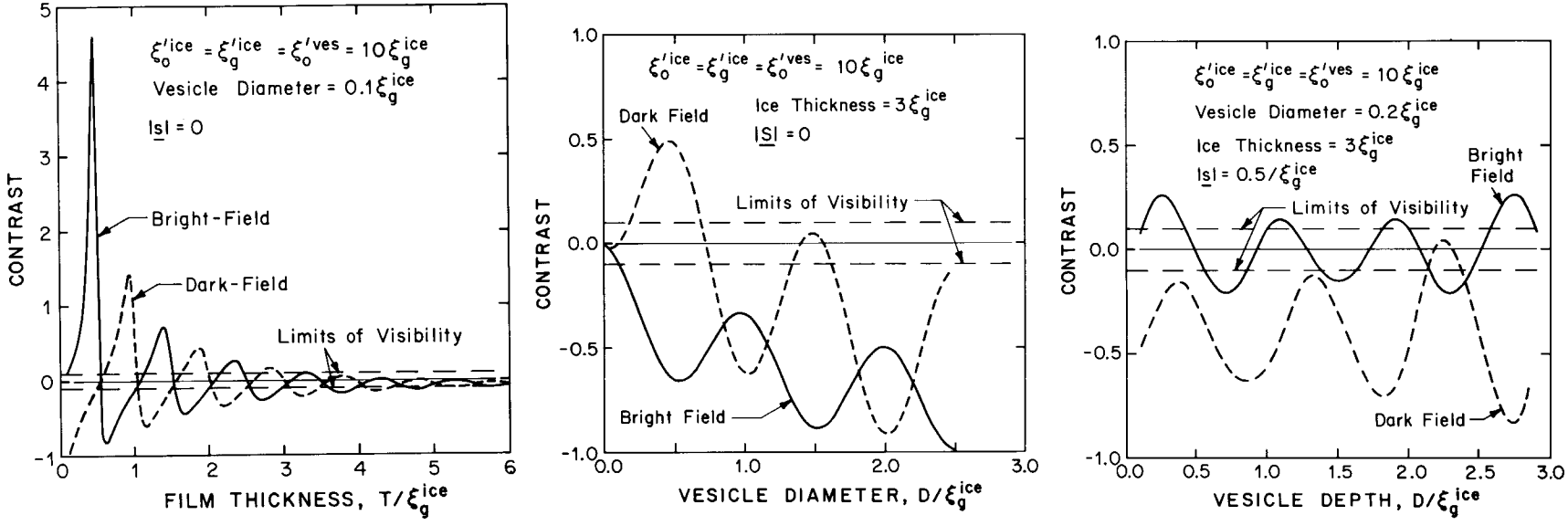

Fig. 6. Bright-field and dark-field contrast profiles for the image of a vesicle located in the middle of ice crystals of increasing thickness. Vesicles appear dark or light, depending on the thickness of the crystal in which they are embedded.

Fig. 7. Contrast profiles for the images of vesicles as a function of their size in an ice crystal oriented at the exact Bragg condition, $|s| = 0$.

Fig. 8. Contrast at the center of the image of a vesicle as a function of the particle depth in a uniform ice crystal.

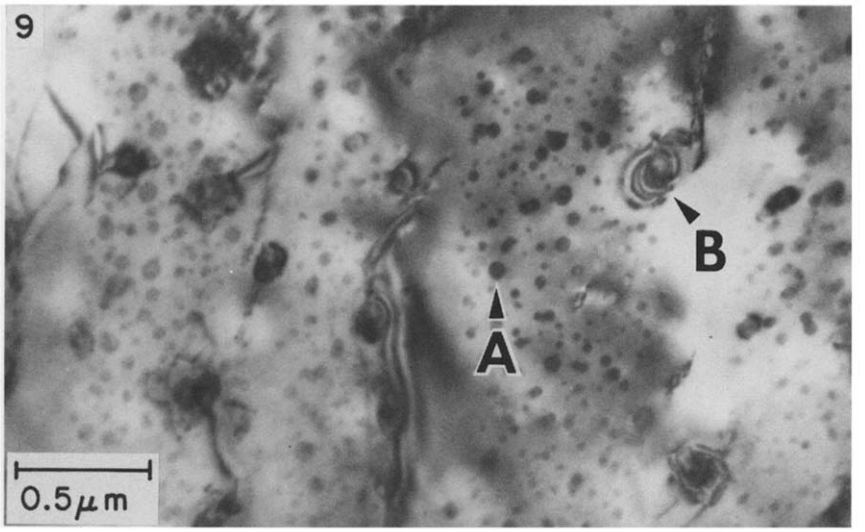

Fig. 9. Bright-field transmission electron microscope image of a frozen, hydrated 1% SHBS, 0.1% CsCl brine vesicular dispersion. Numerous stained vesicles are present (A). Some particles induce strain fields in the ice matrix that produce bands of contrast (B) in the image.

creases when uranyl groups (UO_2^{2+}) replace Na^+ counterions that are ionically bound to negatively charged surfactant head-groups. Other stains may be better suited to SHBS systems. For example, CsCl can be used instead of NaCl in SHBS-brine systems, or Na^+ in SHBS can be replaced with Cs^+. Cesium not only serves as a positive stain but is akin to the ions in SHBS systems. For cationic amphiphiles, the iodide ion can play a similar role. Fig. 9 is an example from a CsCl-stained SHBS vesicular system.

Bands of contrast are seen around some of the particles in Fig. 9. These are similar to the contours which surround polystyrene spheres and small liquid-crystallites in ice [26]. Crystals which precipitate from freezing aqueous uranyl acetate, sodium chloride and cesium chloride solutions also produce contours in the ice around them [26]. The contrast bands are sensitive to tilt and sometimes display lines along which there is no contrast [37]. The bands therefore are likely caused by strain fields created by differential expansion of ice and the inclusion when the sample solidifies.

Effects of radiolysis on frozen, hydrated systems

Radiation by the electron beam modifies the morphology of frozen specimens. Talmon [43] recently reviewed this topic. During irradiation of pure hexagonal ice, cavities form [36,44] and mass is lost [27]. Frozen oleic phases lose their crystallinity and crosslink when bombarded by high-energy electrons [25], as do other crystalline biological [45] and polymeric [46] materials. Frozen, hydrated vesicular samples also suffer radiation damage. Fig. 10a shows a 1% SHBS, 1% uranyl acetate vesicular dispersion which received the minimum electron dose needed to locate, focus, and record its image (approx. $3 \cdot 10^2$ C/m^2 at this magnification). Fig. 10b is the same area after it received $3 \cdot 10^3$ C/m^2. During radiolysis, some particles (A), that were invisible in Fig. 10a, were revealed.

There are at least three mechanisms which can account for vesicles being 'exposed' by radiolysis: (1) when mass is lost, the ice crystal shifts to a new orientation for which the contrast of inclusions is greater (Fig. 3); (2) when mass is lost, the specimen thins and vesicles of previously low contrast in thick crystals reveal themselves (Fig. 6 shows a particle to be invisible when the ice crystal thickness is above $4\xi_g^{ice}$); (3) vesicles physically expand – possibly because they are attacked by the free radicals that are generated in ice when it is irradiated – the contrast of larger vesicles often being

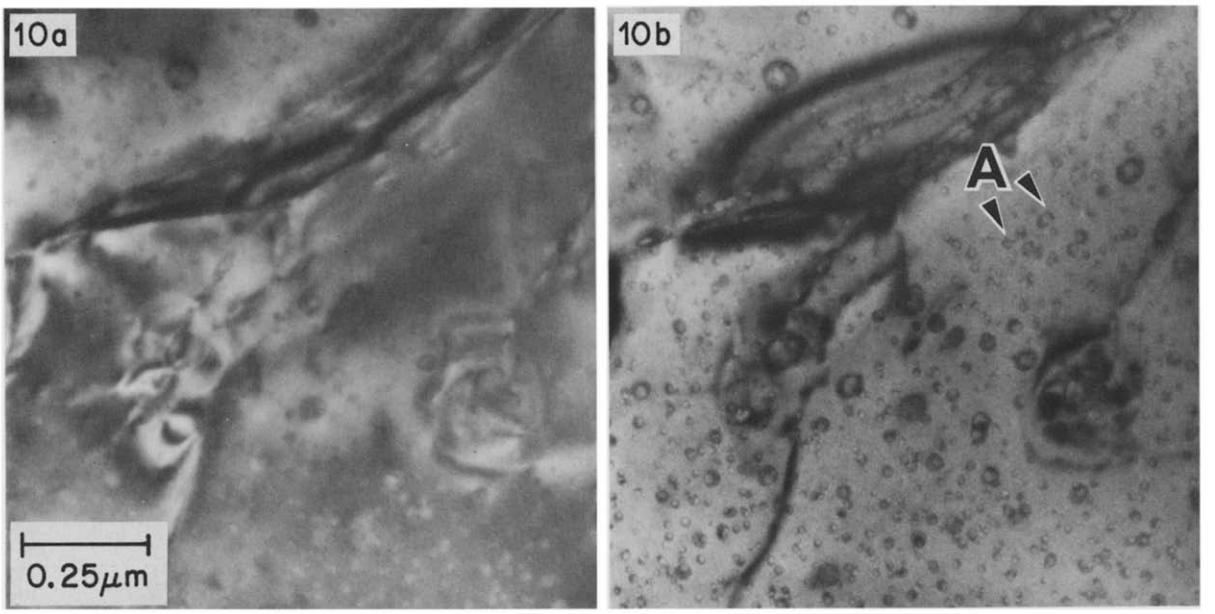

Fig. 10. a. Bright-field image of a 1% SHBS, 1% uranyl acetate vesicular dispersion that was recorded with about $3 \cdot 10^2$ C/m^2. b. Area in Fig. 10a after receiving $3 \cdot 10^3$ C/m^2. During radiolysis some vesicles (A) were revealed.

greater than that of smaller ones (Fig. 7).

All of these mechanisms may contribute to vesicles being revealed during radiolysis. Images of vesicles in ice do appear to expand while being irradiated [24]. Fig. 1b is an example. During radiolysis, many vesicle images, for example at B in Fig. 1b, expand. Areas of lower contrast also form on vesicles (C) and some particles appear lighter (D) or disappear as the sample is irradiated.

Diffraction contrast theory can explain vesicle images expanding if the cause is thinning of ice. Fig. 11a shows how the contrast varies over the projected area of a vesicle image in a thick ice crystal. Due to insufficient contrast, this particle appears to be only 60% of its actual size. Fig. 11b shows the contrast profile for the same vesicle in a thinner crystal. The inclusion now appears to have a diameter of 80% of the actual value. Fig. 11a and b also shows that stained vesicles display greater contrast in thick ice crystals than do unstained ones. Although a vesicle image can appear smaller than the particle itself, an in-focus image of an inclusion that does not produce a strain field in the crystal cannot be larger than the particle actually is.

So far, it has not been possible to determine which mechanism accounts for the effects of radiation on frozen vesicular dispersion. However, the distributions of vesicle sizes in micrographs imaged with minimum radiation dose agree best with small-angle X-ray scattering measurements from unfrozen samples [24]. In addition, vesicle boundaries in transmission electron microscopic images are always well defined, even in images formed with minimum radiation dose (cf. those vesicles visible in Fig. 10a and b). This suggests that vesicles in frozen, hydrated specimens physically expand during radiolysis.

Structure in stained, freeze-dried vesicular dispersions

One advantage of cold-stage microscopy is that drying artifacts [12] are avoided. Fig. 12 shows an air-dried, sonicated 0.07% bovine phosphatidylcholine, 0.1% uranyl acetate dispersion. The contrast fringes in Fig. 12 are not restricted to well-defined particles. These structures differ from those in a thermally fixed sample (compare Fig. 12 with Figs. 2 and 13a).

A frozen, hydrated specimen cal also be freeze-dried in situ, as Heide and Grund [47] have dem-

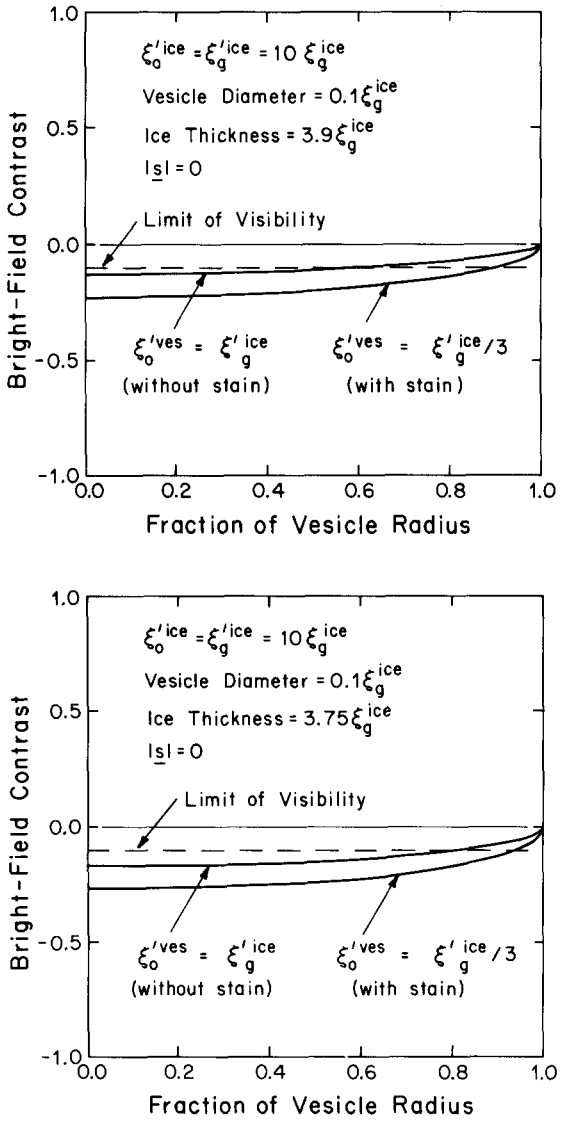

Fig. 11. a. Variation of contrast over the projected images of unstained and stained vesicles in a thick ice crystal. The unstained vesicle appears to have a diameter of only 60% of its actual value. b. Appearance of vesicles with and without stain in a crystal thinner than the one in a. More of the unstained vesicle is visible in the thinner crystal.

onstrated. This is done by elevating the sample temperature to about 198 K. At this temperature, ice sublimes slowly in the microscope because its vapor pressure is $9 \cdot 10^{-4}$ Torr [48]. As ice sublimes from thin specimen areas, small holes, which are hexagonal in shape, first form and enlarge gradually as additional material leaves. Within a few minutes, all of the volatile material is gone and a freeze-dried vesicular dispersion remains. Structures in thin areas stay in their positions during freeze-drying and do not change further when they are warmed to room temperature in the microscope.

Fig. 13a shows a sonicated 0.07% bovine phosphatidylcholine, 0.1% uranyl acetate dispersion in the frozen state, imaged with minimum radiation. Fig. 13b is the same field of view after in situ freeze-drying at 198 K. Structure in the freeze-dried specimen matches that in the frozen, hydrated state. However, vesicles such as those at A shrink during freeze-drying as do other frozen, hydrated biological materials (cf. Boyde and Franc [49]).

Some of the objects in Fig. 13 are likely to be liquid-crystalline particles which survived sonication of the dispersion; compare Fig. 14 which shows a hydrated/freeze-dried pair of bright-field micrographs from an unsonicated 0.07% bovine phosphatidylcholine, 0.1% uranyl acetate dispersion. The micrograph of the frozen, hydrated sample, Fig. 14a, reveals a structural pattern indicative of the Dupin cyclides [50] prevalent in both biological and synthetic smectic, lyotropic liquid crystallites (Ref. 51; Zasadzinski, J.A., unpublished data). The freeze-dried sample, Fig. 14b, lacks evidence of the cyclide.

Ice is the main source of the free radicals that damage a frozen, hydrated specimen during radiolysis [43]. Because ice is lost, a freeze-dried sample is less sensitive to radiation damage and can be imaged at higher magnifications. Fig. 13c is an in-focus, high-magnification micrograph of part of Fig. 13b. The irregular particle on the right-hand side of Fig. 13c displays mass-thickness contrast fringes that follow the outer particle contour. The spacing of these fringes and those on similar particles is about 3.6 nm, but whether the fringes represent surfactant bilayers cannot be decided because the freeze-drying process may have altered them.

Fig. 15 shows the same freeze-dried vesicle at two tilt angles: $-20°$ (Fig. 15a) and $+45°$ (Fig. 15b). The apparent diameter of the vesicle (its projection onto the image plane) changes. This and tilt experiments on other particles suggest that vesicles collapse slightly when the volatile compo-

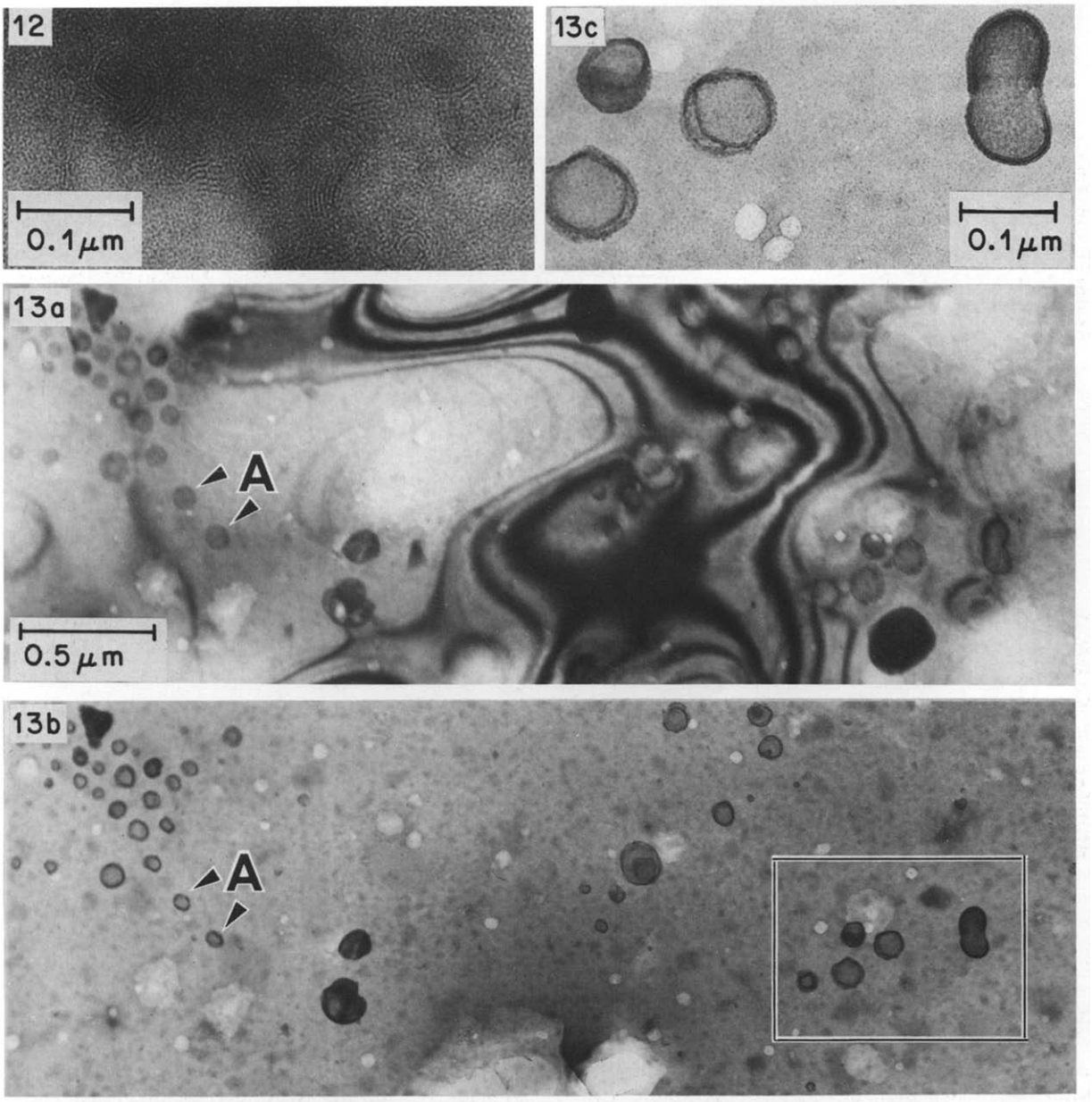

Fig. 12. Air-dried 0.07% bovine phosphatidylcholine, 0.1% uranyl acetate vesicular dispersion imaged with the objective lens defocussed −1.1 μm. Drying produces structure (A) not present in thermally fixed specimens.

Fig. 13. a. Bright-field micrograph of a sonicated 0.07% bovine phosphatidylcholine, 0.1% uranyl acetate dispersion in the frozen, hydrated state. b. Same field of view as in a after the sample has been freeze-dried in the microscope at 198 K. Vesicles are smaller after freeze-drying (compare those at A). c. Enlarged view of part of b.

nents in the dispersion sublime. Radiation damage prevents imaging frozen, hydrated vesicles at magnifications as high as those of Fig. 13c or Fig. 15.

Structure in thicker regions of frozen, hydrated specimens is not always preserved during freeze-drying. In thicker areas, ice appears to leave the

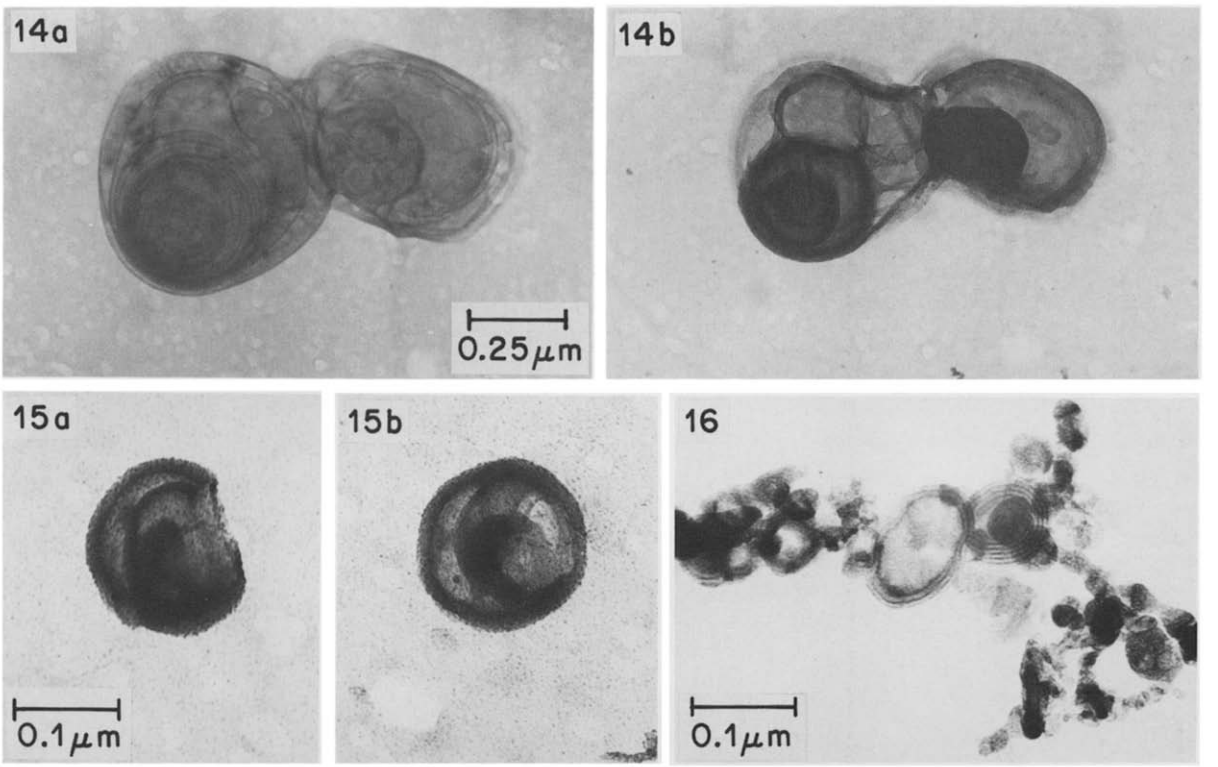

Fig. 14. a. Transmission electron microscope bright-field image of an unsonicated, frozen, hydrated 0.07% bovine phosphatidylcholine, 0.1% uranyl acetate liquid-crystalline dispersion. b. Area in a after it has been freeze-dried in situ at 198 K.

Fig. 15. a. Micrograph of a freeze-dried particle in a 0.07% bovine phosphatidylcholine, 0.1% uranyl acetate dispersion. Stage tilt is −20°. b. Area a, stage tilt +45°.

Fig. 16. Structure from a thick area of a frozen, hydrated 0.07% bovine phosphatidylcholine thin, 0.1% uranyl acetate vesicular dispersion that was freeze-dried in situ.

sample along a receding front which can sweep material along with it. This action agglomerates vesicles and moves them away from their original positions in a sample. Fig. 16 exemplifies the structures that form during freeze-drying of thicker sample areas.

Conclusions

Fast-freeze, cold-stage microscopy reveals structure in aqueous vesicular dispersions. The method makes unstained vesicles of natural or synthetic amphiphiles visible in their natural, hydrated state. The contrast mechanisms responsible for images of frozen, hydrated vesicle systems are explained by the dynamical theory of electron diffraction [33]. Measurements of average vesicle diameters in images of frozen, hydrated samples that have received a minimum amount of radiation from the electron beam are in accord with those from quasi-elastic light-scattering and small-angle X-ray scattering from similar, unfixed, room temperature dispersions [24].

Radiation damage and positive stains enhance contrast in transmission electron microscopic images of frozen, hydrated vesicular dispersions, but both change vesicle structure. Radiolysis by the electron beam causes images of vesicles em-

bedded in ice to enlarge and creates areas of lower contrast on them. On the other hand, adding positive stains such as uranyl acetate or cesium chloride reduces the size of SHBS vesicles [24].

When stain is present, vesicular dispersions freeze-dried in situ can be viewed in the microscope. In situ freeze-drying is preferred over conventional freeze-drying methods because samples are fixed at higher cooling rates, the freeze-drying process can be observed as well as controlled, and images of the specimen in the hydrated and dried states can be compared. In thin specimen areas, structure in freeze-dried vesicular dispersions resembles that in the frozen, hydrated state, although vesicles shrink and sometimes partially collapse when they are freeze-dried. Thereafter, warming to room temperature does not affect them.

Vesicle samples for cold-stage microscopy are affected by radiolysis, stain, and freeze-drying. The mechanisms responsible for changes brought about by fixing and irradiating aqueous vesicular dispersions are not yet clear but must be understood before images of complex structured fluids such as micellar solutions and microemulsions can be fully interpreted.

Acknowledgments

This research was supported by grants from the Fossil Energy Division of the U.S. Department of Energy, from the Unites States-Israel Binational Science Foundation (BSF), Jerusalem, Israel, and from the Office of International Programs, University of Minnesota. We thank E.W. Kaler for light-scattering and X-ray scattering measurements and J.A. Zasadzinski for identifying Dupin cyclides in frozen, aqueous dispersions of bovine phosphatidylcholine.

References

1 Huang, C.-H. (1969) Biochemistry 8, 344–352
2 Papahadjopoulos, D. (ed.) (1978) Ann. Acad. Sci. 308, 1–462
3 Deguchi, K. and Mino, J. (1978) J. Colloid Interface Sci. 65, 155–161
4 Finkelstein, M. and Weissman, G. (1978) J. Lipid Res. 19, 289–303
5 Puig, J.E., Franses, E.I., Talmon, Y., Davis, H.T., Miller, W.G. and Scriven, L.E. (1982) Soc. Pet. Eng. J., 22, 37–52
6 Horne, R.W. and Whittaker, V.P. (1962) Z. Zellf. 58, 1–16
7 Finean, J.B. and Rumsby, M.G. (1963) Nature 197, 1326–1327
8 Horne, R.W., Bangham, A.D. and Whittaker, V.P. (1963) Nature 200, 1340
9 Bangham, A.D. and Horne, R.W. (1964) J. Mol. Biol. 8, 660–668
10 Papahadjopoulos, D. and Miller, N. (1967) Biochim. Biophys. Acta 135, 624–638
11 Glauert, A.M. and Lucy, J.A. (1969) J. Microsc. 118, 401–408
12 Talmon, Y. (1982) J. Colloid Interface Sci., submitted
13 Johnson, S.M., Bangham, A.D., Hill, M.W. and Korn, E.D. (1971) Biochim. Biophys. Acta 233, 820–826
14 Skarnulis, A.J., Strong, P.J. and Williams, R.J.P. (1978) J. Chem. Soc. Chem. Commun. 1030–1032
15 Mann, S., Skarnulis, A.J. and Williams, R.J.P. (1979) J. Chem. Soc. Chem. Commun. 1067–1068
16 Miyamoto, V.K. and Stoeckenius, W. (1971) J. Membrane Biol. 4, 252–269
17 Taylor, K.A. (1978) J. Microsc. 112, 115–125
18 Forge, A., Knowles, P.F. and Marsh, D. (1978) J. Membrane Biol. 41, 249–263
19 Van Venetië, R., Leunissen-Bijvelt, J., Verkleij, A.J. and Ververgaert, P.H.J.Th. (1980) J. Microsc. 118, 401–408
20 Bachman, L. and Schmitt, W.W. (1971) Proc. Natl. Acad. Sci. U.S.A. 68, 2149–2152
21 Van Venrooij, G.E.P.M., Aertsen, A.M.H.J., Hax, W.M.A., Ververgaert, P.H.J.Th., Verhoeven, J.J. and Van der Vorst, H.A. (1975) Cryobiology 12, 46–61
22 Talmon, Y., Davis, H.T., Scriven, L.E. and Thomas, E.L. (1979) Rev. Sci. Instr. 50, 698–704
23 Talmon, Y., Davis, H.T., Scriven, L.E. and Thomas, E.L. (1980) In Proceedings of the 7th European Congress on Electron Microscopy (Brederoo, P. and dePriester, W., eds.), Vol. II, pp. 718–719, 7th Eur. Congr. Foundn., Leiden
24 Kaler, E.W., Falls, A.H., Davis, H.T., Scriven, L.E. and Miller, W.G. (1982) J. Colloid Interface Sci., in the press
25 Talmon, Y. (1979) Ph.D. Thesis, University of Minnesota
26 Falls, A.H. (1982) Ph.D. Thesis, University of Minnesota
27 Talmon, Y., Davis, H.T., Scriven, L.E. and Thomas, E.L. (1979) J. Microsc. 117, 321–332
28 Talmon, Y. and Miller, W.G. (1978) J. Colloid Interface Sci. 67, 284–291
29 Buscall, R. and Ottewill, R.H. (1975) in Specialist Periodical Report, Colloid Science (Everett, D.H., ed.), Vol. 2, pp. 191–245, The Chemical Society, London
30 Perlov, G. and Talmon, Y. (1982) Rev. Sci. Instr., submitted
31 Franses, E.I. (1979) Ph.D. Thesis, University of Minnesota
32 Puig, J.E. (1982) Ph.D. Thesis, University of Minnesota
33 Howie, A. and Whelan, M.J. (1961) Proc. R. Soc. London A 263, 217–237
34 Hanszen, K.-J. (1971) in Advances in Optical and Electron Microscopy (Barer, R. and Cosslett, V.E., eds.), Vol. 4, pp. 1–84, Academic Press, London
35 Handlin, D.L. (1981) in Proceedings of the 39th Annual EMSA Meeting (Bailey, G.W., ed.), pp. 338–339, Claitor, Baton Rouge

36 Falls, A.H. (1982) in Proceedings of the 40th Annual EMSA Meeting, in the press
37 Ashby, M.F. and Brown, L.M. (1963) Phil. Mag. 8, 1649–1676
38 Van Landyut, J., Gevers, R. and Amelinckx, S. (1965) Phys. Stat. Sol. 10, 319–335
39 Rühle, M.R. (1972) in Radiation Induced Voids in Metals (Corbett, J.W. and Ianiello, L.C., eds.), pp. 255–291, U.S. Atomic Energy Commission, Oak Ridge, TN
40 Humphries, C.J. and Hirsch, P.B. (1968) Phil. Mag. 18, Ser. 8, 115–122
41 Thomas, G. and Goringe, M.J. (1979) Transmission Electron Microscopy of Materials, pp. 141, 239, Wiley, New York
42 Nicholas, J.F. (1966) Acta Crystallogr. 21, 880–881
43 Talmon, Y. (1982) J. Microsc. 125, 227–237
44 Unwin, P.N.T. and Muguruma, J. (1972) Phys. stat. Sol. (a) 14, 207–216
45 Cosslett, V.E. (1978) J. Microsc. 113, 113–129
46 Grubb, D.T. (1974) J. Materials Sci. 9, 1715–1736
47 Heide, H.G. and Grund, S. (1974) J. Ultrastruct. Res. 48, 259–268
48 Washburn, E.W., ed. (1928) International Critical Tables of Numerical Data, Physics, Chemistry and Technology, Vol. 3, p. 210, McGraw-Hill, New York
49 Boyde, A. and Franc, F. (1981) J. Microsc. 122, 75–86
50 Friedel, M.G. (1922) Ann. Phys. 18, 273–483
51 Kléman, M., Williams, C.E., Costello, M.J. and Gulik-Krzywicki, T. (1977) Phil. Mag. 35, 33–56